



# Projecting the future vegetation–climate system over East Asia and its RCP-dependence

Weiguang Liu<sup>1,2</sup> · Guiling Wang<sup>2</sup> · Miao Yu<sup>1</sup> · Haishan Chen<sup>1</sup> · Yelin Jiang<sup>2</sup> · Meijian Yang<sup>2</sup> · Ying Shi<sup>3</sup>

Received: 23 August 2019 / Accepted: 7 August 2020  
© Springer-Verlag GmbH Germany, part of Springer Nature 2020

## Abstract

The future vegetation–climate system over East Asia, as well as its dependence on Representative Concentration Pathways (RCPs), is investigated using a regional climate–vegetation model driven with boundary conditions from Flexible Global Ocean–Atmosphere–Land System Model: Grid-point Version 2. Over most of the region, due to the rising CO<sub>2</sub> concentration and climate changes, the model projects greater vegetation density (leaf area index) and gradual shifts of vegetation type from bare ground to grass or from grass to trees; the projected spatial extent of the vegetation shift increases from RCP2.6 to RCP8.5. Abrupt shifts are projected under RCP8.5 over northeast China (with grass replacing boreal needleleaf evergreen trees due to heat stress) and India (with tropical deciduous trees replacing grass due to increased water availability). The impact of vegetation feedback on future precipitation is relatively weak, while its impact on temperature is more evident, especially during DJF over northeast China and India with differing mechanisms. In northeast China, the projected forest loss induces a cooling through increased albedo, and daytime high temperature ( $T_{\max}$ ) is influenced more than nighttime low temperature ( $T_{\min}$ ); in India, increased vegetation cover induces an evaporative cooling that outweighs the warming effect of an albedo decrease in DJF, leading to a weaker impact on  $T_{\max}$  than on  $T_{\min}$ . Based on a single model, the qualitative aspects of these results may hold while quantitative assessment will benefit from a follow-up regional model ensemble study driven by multiple general circulation models.

**Keywords** Vegetation–atmosphere interactions · Coupled models · Regional models · Climate change · East Asia

---

**Electronic supplementary material** The online version of this article (<https://doi.org/10.1007/s00382-020-05411-2>) contains supplementary material, which is available to authorized users.

---

✉ Guiling Wang  
guiling.wang@uconn.edu

<sup>1</sup> Key Laboratory of Meteorological Disaster, Ministry of Education/International Joint Research Laboratory on Climate and Environment Change/Collaborative Innovation Center on Forecast and Evaluation of Meteorological Disasters, Nanjing University of Information Science and Technology, Nanjing 210044, China

<sup>2</sup> Department of Civil and Environmental Engineering, and Center for Environmental Science and Engineering, University of Connecticut, Storrs, CT 06269, USA

<sup>3</sup> National Climate Center, China Meteorological Administration, Beijing 100081, China

## 1 Introduction

Both the Earth's climate and the global ecosystems are undergoing unprecedented changes (IPCC 2013; Bonan and Doney 2018). The interactions between climate and terrestrial ecosystems have been recognized as one of the major uncertainties in climate change predictions (Melillo et al. 1993; Cramer et al. 2001; Franklin et al. 2016; Duveiller et al. 2018). On one hand, vegetation changes can modulate the exchanges of water, energy, and momentum between land and atmosphere through biogeophysical and biogeochemical processes (Bonan 2008; Li et al. 2015; Alkama and Cescatti 2016), thus modifying regional and global climate (Wang et al. 2004, 2016, 2017; Zhou et al. 2007; Peng et al. 2013; Shen et al. 2015). The local impacts of vegetation–atmosphere interactions are dependent on vegetation type, geographical location and background climate (Bonan 2008; Jeong et al. 2009a, b; Duveiller et al. 2018). Degradation of vegetation coverage may result in a decrease in evaporative cooling in the Tropics, which can

further enhance warming (Henderson-Sellers et al. 1993; Gibbard et al. 2005), whereas the degradation-induced surface albedo increase may cause a cooling especially at high latitudes (Betts 2000; Notaro and Liu 2008). On the other hand, climate (e.g., temperature, rainfall, and solar radiation) can influence the growth, competition, and thus geographical distribution of vegetation (Nemani et al. 2003; Zhao et al. 2019). Under increasing greenhouse gas (GHG) concentrations and temperature, a positive trend (i.e., greening) of leaf area index (LAI) was observed globally (Zhu et al. 2016). However, in projecting future vegetation changes, the CO<sub>2</sub> fertilization and climate change impacts may not always be consistent and complications can stem from climate change altering resource competition among different vegetation types (Yu et al. 2014).

After Charney's (1975) pioneering hypothesis on Sahel desertification, many modeling and observational studies explored the positive feedbacks between vegetation and rainfall (Xue and Shukla 1993; Zeng et al. 1999; Wang and Eltahir 2000a, b; Wang et al. 2004; Yu et al. 2017). As the effects of vegetation on climate are difficult to establish directly through observations (Bonan 2008), global general circulation models (GCMs) have been used as primary tools to investigate global vegetation–climate feedback (Cox et al. 2000; Davin and de Noblet-Ducoudré 2010; Ma et al. 2013; Mao et al. 2016). On this aspect, modeling studies by Xue et al. (2010) and Notaro et al. (2011) both showed that vegetation biophysical processes can exert feedbacks on the monsoon regions and East Asia is one of the most influenced. To address the limitation of the GCMs' coarse resolution (which is especially problematic for East Asia due to the complex terrain, Gao et al. 2006), regional climate models have been used to study the role of land use–land cover changes as a driver for regional climate changes. Past studies on afforestation and deforestation supported a consensus that expanded vegetation cover tends to cause greater evapotranspiration (ET) and rainfall (Liu et al. 2008; Yu et al. 2013; Ma et al. 2013; Wei et al. 2017) with spatially heterogeneous responses across China. Notaro et al. (2017), using a regional climate model with observed LAI, found that greater LAI leads to greater latent heat flux (and a modest decrease in sensible heat flux), while Notaro et al. (2011) found that both sensible and latent heat fluxes increase as a result of higher forest cover and LAI simulated by the Community Climate System Model (CCSM) over China. Through comparing vegetation fraction variation over eastern China, Yan et al. (2019) illustrated that an increase in LAI dampens warming, and the effect is stronger in the growing season. These past studies suggested that the effects of vegetation–climate feedback should be accounted for in climate variability and climate change studies.

Climate change is expected to cause serious socio-economic consequences globally. East Asia is especially

vulnerable to climate changes due to the large population (Hua et al. 2017), and many studies have been conducted to investigate climate change and extremes in this region (Zou and Zhou, 2013; Shi et al. 2017; Li et al. 2018). Future climate change is expected to significantly influence the terrestrial ecosystems, including for example a shift from evergreen to drought deciduous trees in the tropics and a poleward shift of forests in mid- and high-latitudes (e.g., Williams et al. 2007; Alo and Wang 2008; Yu et al. 2014), an increase of LAI over most of the globe (Mahowald et al. 2016; Tharammal et al. 2018), and an expansion of forest and bare ground at the expense of grassland (Gang et al. 2017). The climate-induced vegetation changes necessarily will influence future regional and global climate. However, despite the documented influence of vegetation cover on East Asian climate, most regional climate studies prescribed vegetation cover and density (e.g., Hua et al. 2015; Li et al. 2017; Niu et al. 2018; Yang et al. 2019); limited by the lack of model capacity to simulate vegetation dynamics or phenology, only a few regional-scale studies over East Asia have accounted for the complex interactions between vegetation and surface climate (Shi et al. 2018; Dan et al. 2015). In this study, using a regional coupled climate–vegetation model, we project future climate and vegetation changes in East Asia, assess their dependence on CO<sub>2</sub> concentration pathways, and evaluate the impact of vegetation feedback on regional climate projections. Section 2 of the paper describes the model, data and experimental design. Model results are presented in Sect. 3. A summary and discussion are given in Sect. 4.

## 2 Model, data and experimental design

### 2.1 Model

The Regional Climate Model Version 4.3.4 (RegCM4.3.4) from the International Centre for Theoretical Physics (Giorgi et al. 2012) coupled with the Community Land Model version 4.5 (CLM4.5, Oleson et al. 2010, 2013), including the carbon–nitrogen (CN) and dynamic vegetation model (DV) submodels (Gotangco Castillo et al. 2012; Yu et al. 2016a), is the primary modeling tool used in this study (RegCM–CLM–CNDV) (Wang et al. 2016). The coupled model has been applied to several regions including West Africa, South America, and Asia (Yu et al. 2016b; Erfanian et al. 2016; Erfanian and Wang 2018; Shi et al. 2018). Specifically for Asia, Shi et al. (2018) evaluated the performance of RegCM–CLM–CNDV in East Asia when forced with boundary conditions from reanalysis data, and documented a reasonable performance in simulating both the climate and vegetation distribution in this region. In comparison to simulations with prescribed vegetation, although the

RegCM–CLM–CNDV produces larger biases in the mean temperature during the winter season, it performs better in simulating the interannual variability of temperature and spatial distribution of mean precipitation. Moreover, for the long-term climate change projection studies, models with dynamic vegetation are a necessity, as changes of vegetation distribution and structure in response to warming and CO<sub>2</sub> concentration changes are expected and may induce substantial impact on the climate.

In this study, we use the same model configuration as Shi et al. (2018) but with a smaller domain. Shi et al. (2018) used the domain from international Coordinated Regional Climate Downscaling Experiment (CORDEX), which is very large and includes a major portion of the western Pacific Ocean. The domain used in the present study is smaller for computational efficiency but is still large enough to include the oceanic forcing. Based on our sensitivity tests, shrinking the domain did not cause noticeable changes in the model performance. The domain covers approximately 10°–60° N, 65°–140° E (Fig. 1) with a horizontal resolution of 50 km, and the model atmosphere includes 18 sigma levels with the top set to 50 hPa. The model physics packages include the radiative transfer scheme from the Community Climate Model version 3 (Kiehl et al. 1996), the planetary boundary layer scheme from Holtslag et al. (1990), and the cumulus convection scheme from Emanuel (1991). More details of the coupled model can be found in Wang et al. (2016) and Shi et al. (2018).

## 2.2 Data

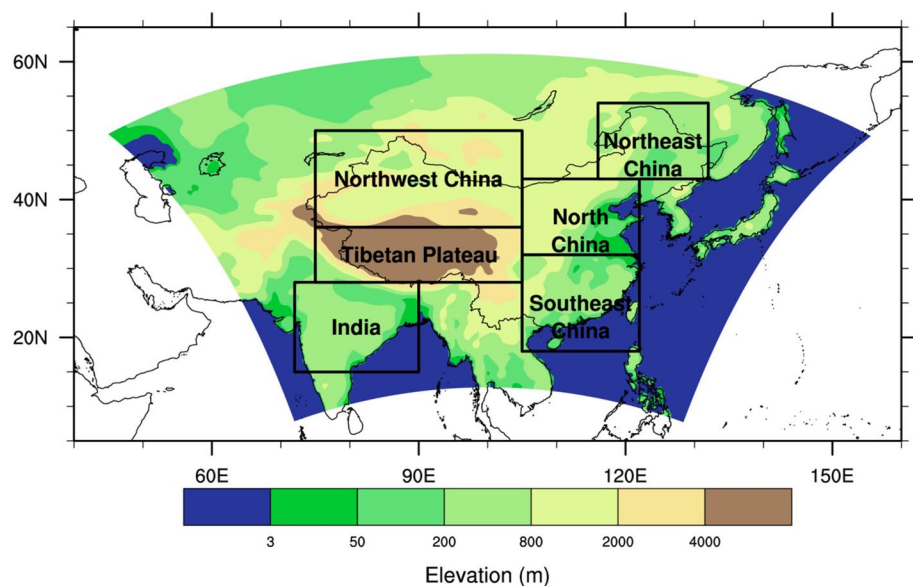
Three Representative Concentration Pathways (RCP) are included in this study which correspond to different CO<sub>2</sub> concentrations that produce a global radiative forcing of 2.6,

4.5 and 8.5 W m<sup>-2</sup> by the end of the 21st century (IPCC, 2013; Moss et al. 2010), representing low (RCP2.6), medium (RCP4.5), and high (RCP8.5) emission scenarios, respectively (Taylor et al. 2012). The atmospheric initial conditions and boundary conditions (ICBC) for the regional model were derived from CMIP5 historical and future simulations from the Flexible Global Ocean–Atmosphere–Land System Model: Grid-point Version 2 (FGOALS-g2) (Li et al. 2013). As a CMIP5 participant from East Asia, FGOALS-g2 model shows a strong capability in simulating East Asia climate (Zhou et al. 2013) and has been used as the boundary conditions by many regional climate projection studies focused on East Asia (e.g., Wang and Chen 2014; He and Zhou 2015; Li et al. 2016, 2018). In addition, Yu et al. (2014) evaluated the vegetation simulation by CLM–CN–DV driven with climates from 19 GCMs, and compared the simulated present-day vegetation distribution with Moderate Resolution Imaging Spectroradiometer (MODIS) satellite data. Based on their results, the simulated vegetation driven with the FGOALS-g2 climate is generally in the middle of the ensemble and close to the ensemble mean.

## 2.3 Experimental design and analysis

Four main pairs of experiments were conducted, corresponding to the historical and three RCP scenarios; each pair consists of two simulations, one using the full RCM–CLM–CNDV model and the other using RCM–CLM with static vegetation. The RCM–CLM simulations are included here to help interpret results from the RCM–CLM–CNDV and to assess vegetation–climate feedback. The two types of simulations share the same model configuration and ICBCs, but differ in how vegetation is treated. In the RCM–CLM–CNDV simulations, the model

**Fig. 1** The topography (shaded, units: m) and sub-regions of the model domain. The boxes illustrate six sub-regions: northwest China (36°–50° N, 75°–105° E), Tibetan Plateau (28°–36° N, 75°–105° E), northeast China (43°–54° N, 116°–132° E), north China (32°–43° N, 105°–122° E), southeast China (18°–32° N, 105°–122° E), and India (15°–28° N, 72°–90° E)



projects not only regional climate but also vegetation distribution and density. In the RCM–CLM simulations, the CN and DV sub-models are turned off; instead, the fractional coverage of different plant functional types (PFTs) and LAI data derived from MODIS are used to prescribe the spatial distribution of vegetation and the seasonal cycle of LAI (Lawrence and Chase 2007; Lawrence et al. 2011). Both types of simulations are conducted for the historical period of 1979–1999 and for each RCP scenario of 2079–2099, and a CO<sub>2</sub> concentration of 353.8, 425.9, 534.3 and 850.0 ppm was set for the historical, RCP2.6, RCP4.5 and RCP8.5 simulations, respectively. To initialize the carbon, nitrogen, and vegetation conditions in RCM–CLM–CNDV, we follow the approach of Wang et al. (2016) in using the equilibrium state derived from spinning up the offline CLM–CN–DV model driven with atmospheric forcing from the RCM–CLM simulations. The RCM–CLM–CNDV cycled through the 1979–1999 (or 2079–2099 for future) ICBC forcing twice; the first 21-year simulations are then discarded as model spin-up and output from the last 20 years are used for analysis. For the RCM–CLM simulations, the 1st year was devoted to model spin-up and the last 20 years were analyzed in this study.

This experimental design allows us to assess future climate and vegetation changes and to also quantify the impact of vegetation feedback on regional climate under different RCPs. Specifically, for each RCP, two scenarios of climate change can be derived, based on two pairs of runs: one pair from the RCM–CLM with prescribed observed vegetation (Past1 and Future1) and one pair from the RCM–CLM–CNDV with dynamic vegetation (Past2 and Future2). The corresponding climate changes can be defined as  $\Delta 1 = \text{Future1} - \text{Past1}$  and  $\Delta 2 = \text{Future2} - \text{Past2}$ . We attribute the differences between  $\Delta 1$  and  $\Delta 2$  to the impact of vegetation feedback on climate change.

An alternative approach to quantifying the impact of vegetation feedback on climate change is to add another type of future climate simulations with prescribed vegetation (Future3). Specifically, vegetation simulated in Past2 (the past climate run from RCM–CLM–CNDV) is used to prescribe vegetation in a RCM–CLM future run (Future3). We attribute the climate differences between Future2 and Future3 to the impact of vegetation feedback on climate change. To test this alternative approach, we conduct three Future3 experiments (corresponding to the three RCPs) for comparison with the first approach.

Our results analyses focus on climate change signals defined by the differences between two climates. To test the statistical significance of these signals, Student's *t* test was used, and results that are significant at 95% confidence level are marked and discussed. In addition to spatially distributed signals, for detailed analysis based on spatial averages, we follow Li et al. (2018) to divide East Asia into six

sub-regions (Fig. 1), including northwest China (36°–50° N, 75°–105° E), Tibetan Plateau (28°–36° N, 75°–105° E), northeast China (43°–54° N, 116°–132° E), north China (32°–43° N, 105°–122° E), southeast China (18°–32° N, 105°–122° E) and India (15°–28° N, 72°–90° E).

## 3 Results

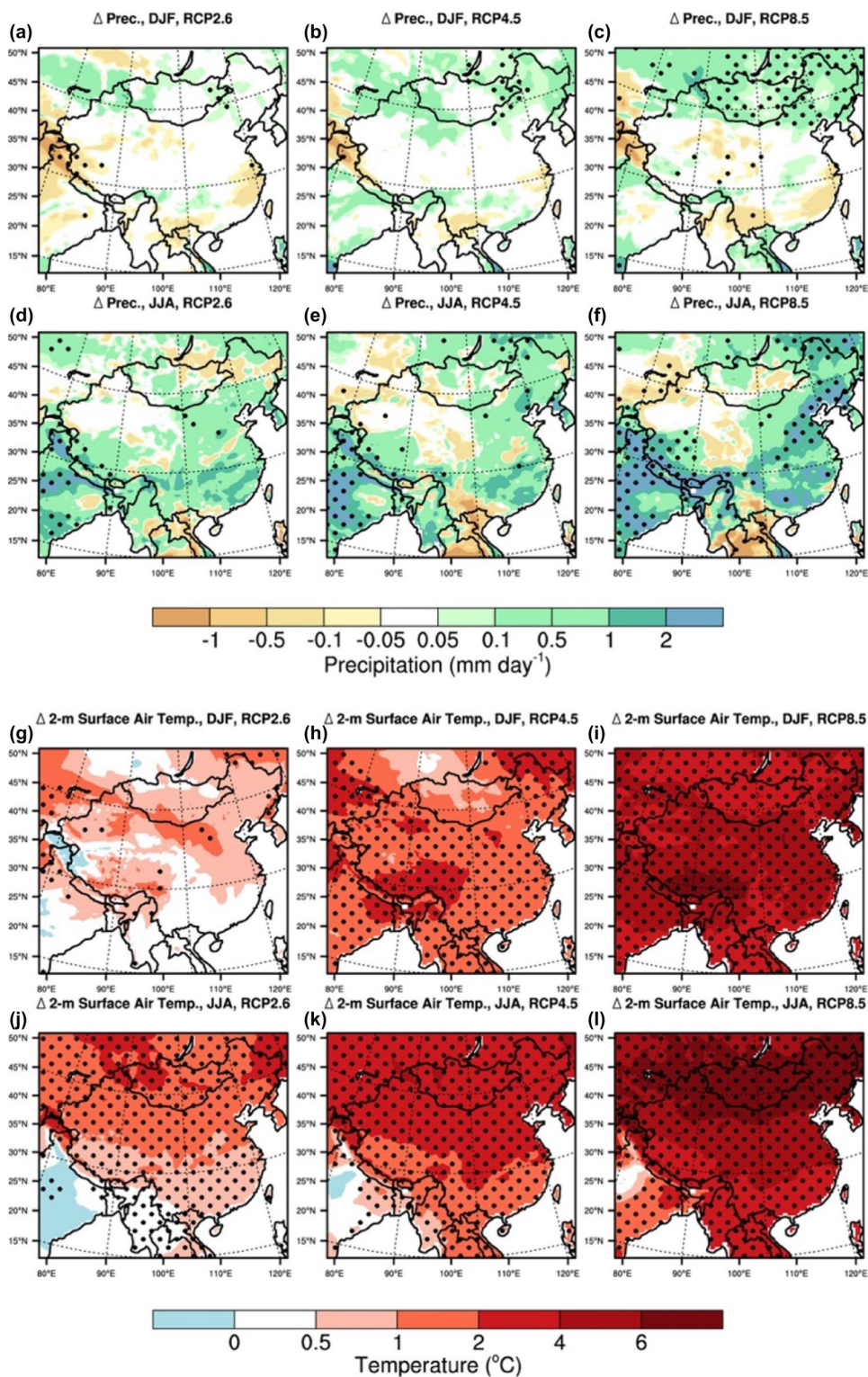
### 3.1 Surface climate change

Shi et al. (2018) evaluated the performance of the RCM–CLM and RCM–CLM–CNDV model in simulating the present-day climate and vegetation in Asia when driven with reanalysis boundary conditions, and found good agreement between the model present-day climate and observations. Therefore this study focuses on future climate projections without detailed validation of the historical simulation.

Compared to the historical simulation, the RCM–CLM model with static vegetation projects an increase of precipitation and temperature over most of the domain (Fig. 2). For precipitation, this increase is dominated by the warm season changes (JJA) (Fig. 2a–c), with negligible contribution from winter (DJF) (Fig. 2d–f); over most of the regions, differences among the three RCPs are rather small. Under all three RCPs, a strong increase of precipitation is projected for the growing season over India, part of Tibetan Plateau, and most of east China including northeast China. The projected increase of temperature is strong for all seasons, and the magnitude of the warming increases from low emission to higher emission scenarios gradually (Fig. 2g–i). An especially strong increase of temperature is projected during the growing season over the mid-latitudes including northeast China, which can induce strong heat stress and may trigger tree mortality. As a result of this exacerbation of growing-season heat stress, when vegetation dynamics is simulated as in the RCM–CLM–CNDV model, a shift from trees to grass is projected for this region, as described in Sect. 3.2.

ET in JJA (warm/wet season) is projected to increase by RCM–CLM with static vegetation, resulting from warming-induced increase of evaporative demand as well as increased water availability due to precipitation increase. The spatial pattern of the projected ET changes (Fig. 3a–f) resembles that of the projected precipitation changes over densely vegetated land during JJA (Fig. 2a–f), and most summertime ET changes are comparable to precipitation changes in magnitude. However, in DJF (winter/dry season), ET changes (Fig. 3a–c) differ remarkably from precipitation changes (Fig. 2a–c), with more ET changes in south China and more precipitation changes in north China. During JJA (summer/wet season), the runoff coefficient (the ratio of runoff to rainfall) is projected to increase over most of the wet

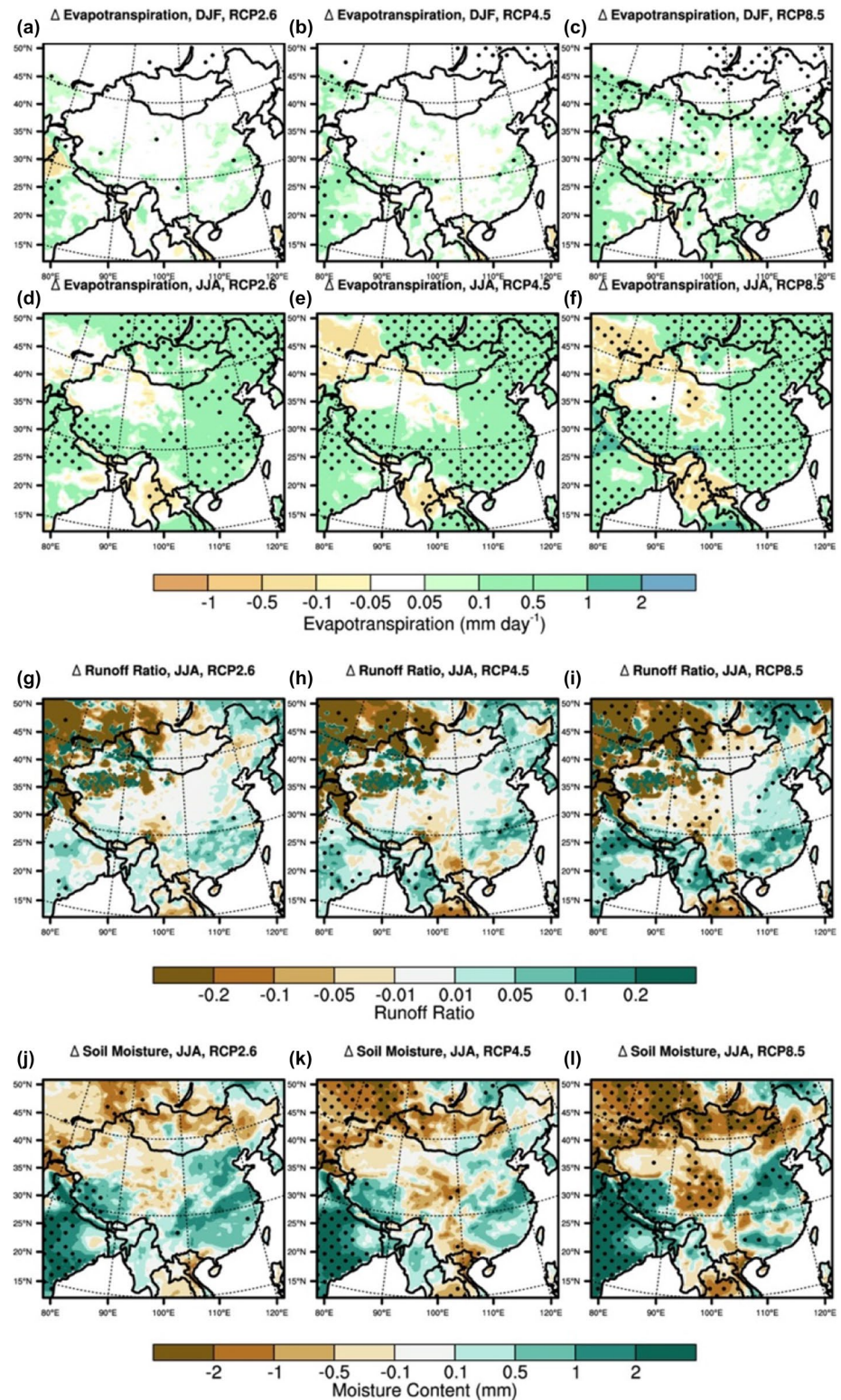
**Fig. 2** Future changes of precipitation (top panel, units:  $\text{mm day}^{-1}$ ) and near surface air temperature (bottom panel, units:  $^{\circ}\text{C}$ ) in DJF (a–c, g–i) and JJA (d–f, j–l) from static vegetation simulations under RCP2.6 (1st column), RCP4.5 (2nd column) and RCP8.5 (3rd column). Areas with values exceeding the two-tailed 95% confidence level with a t distribution are dotted



regions (Fig. 3g–i), as a result of the increase of precipitation intensity and precipitation extremes. Therefore, although precipitation increases, a greater fraction of it runs off as rain rate quickly exceeds the infiltration capacity during heavy precipitation events. As a result of all

changes in precipitation (Fig. 2a–f), ET (Fig. 3a–f) and runoff (Fig. 3g–i), soil is projected to become wetter in north China and India, and drier over the mid-latitudes (including northeast China) and inland China (Fig. 3j–l). In India, the wetter soil conditions persist all year round,

**Fig. 3** Projected future changes of evapotranspiration in DJF and JJA (top panel, units:  $\text{mm day}^{-1}$ ), runoff coefficient (the ratio of runoff to precipitation) in JJA (middle panel, units: 1) and moisture in the top 10 cm soil in JJA (bottom panel, units: mm) under RCP2.6 (1st column), RCP4.5 (2nd column) and RCP8.5 (3rd column). Areas with values exceeding the two-tailed 95% confidence level with a t distribution are dotted



which further influences the surface heat flux changes (in Sect. 3.3). In northeast China, despite the strong increase of precipitation, soil moisture is projected to decrease due to the projected increase of ET and runoff coefficient; the drier soil during the growing season (JJA) can also

contribute to the projected shift of vegetation from trees to grass over northeast China, which will be discussed in the next section.

### 3.2 Vegetation and changes

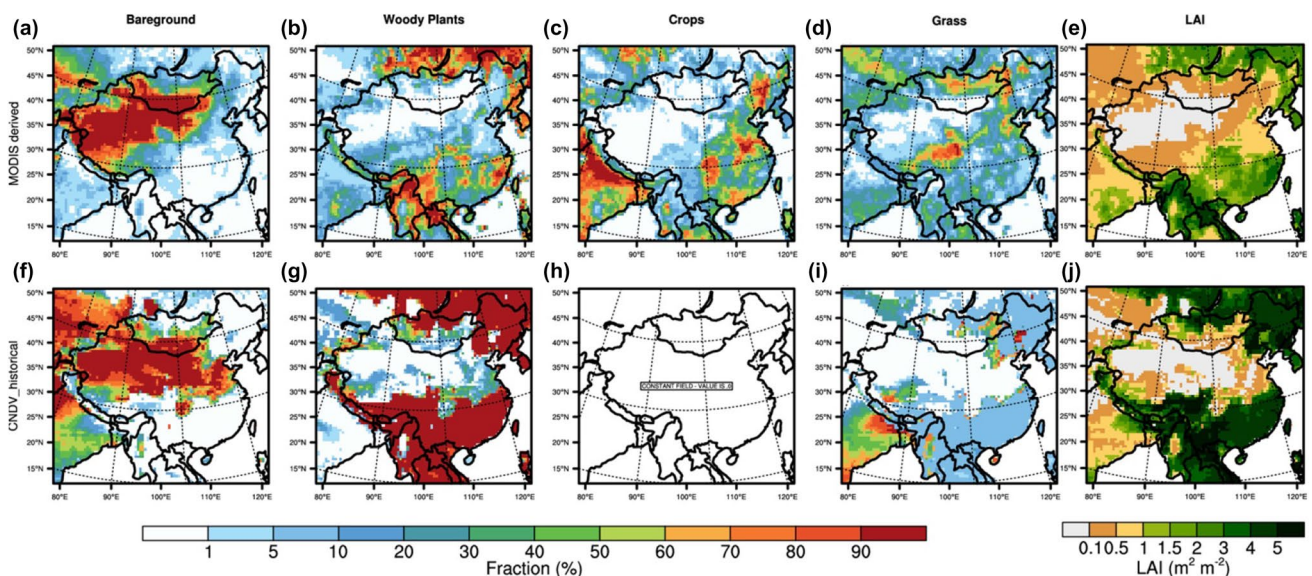
The spatial distribution of natural vegetation from the RCM–CLM–CNDV historical simulation is shown in Fig. 4. Since the model simulates natural ecosystems only, the distribution of cropland (Fig. 4c) has to be kept in mind when comparing the model-simulated vegetation distribution against observations. Indeed, a major discrepancy in PFTs coverage between the model and MODIS data is found over cropland areas, as the model simulates the potential natural vegetation in equilibrium with the local climate over the cropland. This underlies the apparent overestimation of woody plants in agriculture-dominated regions such as northeast China and southeast China (Fig. 4b, g) and overestimation of grassland in India (Fig. 4d, i). The lack of crops in the model is also partly responsible for the vast overestimation of bare ground in north China (Fig. 4a, f). Another cause for the lack of model vegetation in north China is the use of boundary conditions from a GCM, which results in a drier regional climate in comparison to the reanalysis-driven simulations; when driven with boundary conditions from reanalysis data, the same regional model simulates a combination of trees, grass, and bare ground for north China region (Shi et al. 2018). Note that in reality, the North China Plain is mostly cropland with widespread irrigation. The lack of consideration for irrigated crops also contributes to the uncertainty in the climate simulation for this region (Kang and Eltahir, 2018). Over the Tibetan Plateau (Fig. 4a–d, f–i), both bare ground and grass coverage are underestimated while tree coverage is overestimated,

which reflects the model’s limitation in simulating the climate–ecosystem there (Shi et al. 2018) partially due to the scarcity of observational data to inform model parameters and parameterizations.

LAI is significantly overestimated over regions where the model overestimates tree coverage (Fig. 4e, j), especially in southeast China and northeast China. These are also regions of high LAI in observations. The model–data disparity reflects not only an overestimation by the regional model but also underestimation by the MODIS data due to satellite signal saturation at high LAIs (e.g., Murray-Tortarolo et al. 2013). In other regions where LAI is lower, the agreement between the model LAI and MODIS LAI is quite good.

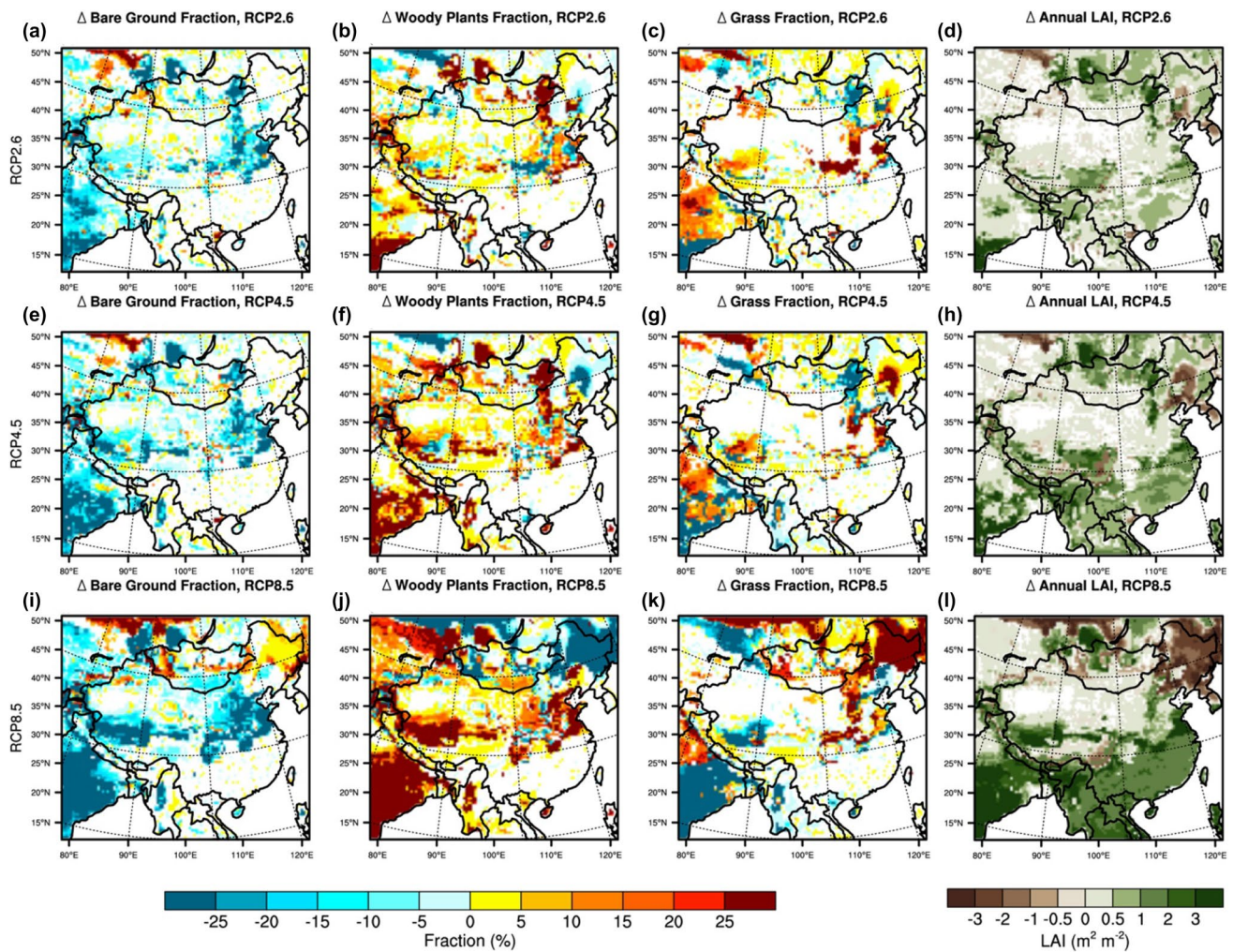
Overall, the RCM–CLM–CNDV can capture the large-scale spatial patterns of typical vegetation distribution and structure. It should be pointed out that the simulation biases documented here result from both deficiency of the coupled regional model and biases of the FGOALS-g2 (which is the source of the RCM boundary conditions) in simulating the large scale atmospheric circulation in this region. When driven by boundary conditions from reanalysis data, the same model performs much better in simulating the present-day vegetation distribution (Shi et al. 2018).

Figure 5 exhibits the projected future changes in vegetation distribution and density. LAI is projected to increase across most of the domain (Fig. 5d–l), indicating denser and greener vegetation in the future. This is qualitatively consistent with numerous studies on future projections (e.g., Alo and Wang 2008; Yu et al. 2016a, b) and with recent observed trend (e.g., Zhu et al. 2016; Zeng et al. 2018; Yao et al. 2019;



**Fig. 4** Coverage (in %) for bare ground, woody plants, crops, and grasses (1st to 4th columns respectively) and the grid-average of annual mean leaf area index (LAI; 5th column, units:  $\text{m}^2 \text{m}^{-2}$ ): from

satellite data used to prescribe vegetation in RCM–CLM (a–e) and from the RCM–CLM–CNDV historical simulation (f–j)



**Fig. 5** Projected future changes of bare ground (a, e, i), woody plants (b, f, j), grass (c, g, k) PFT coverage changes (units: %) and annual mean LAI changes (d, h, l, units:  $\text{m}^2 \text{m}^{-2}$ ) compared to historical

simulations, under RCP2.6 (1st row), RCP4.5 (2nd row) and RCP8.5 (3rd row). Only areas with values exceeding the two-tailed 95% confidence level with a t distribution are shaded

Chen et al. 2019). The projected widespread increase of LAI is partly due to the  $\text{CO}_2$  fertilization effects and partly due to the resulting warmer and wetter climate. In addition, shifts of vegetation types and coverage are also projected for several regions, especially India, Tibetan Plateau, north China, and northeast China. Over India, woody plants (Fig. 5b–j) would expand over both bare ground (Fig. 5a–i) and grassland (Fig. 5c–k). Over the Tibetan Plateau and north China, both tree and grass coverages would expand and bare ground would shrink. Conversely, over northeast China, grassland would expand at the expense of forest, which causes LAI to decrease in this region, a clear exception to an otherwise across-the-board increase of LAI.

To examine the projected vegetation changes in detail, the spatially averaged PFT fraction of each region is compared in Fig. 6. For northwest China (which is mostly bare ground), a slight expansion of vegetation coverage (therefore

a slight decrease of bare ground) is projected. For southeast China (a region with extensive vegetation cover), broadleaf evergreen trees expand at the expense of broadleaf deciduous trees. Three regions (including Tibetan Plateau, north China, and India) would experience a substantial decrease of bare ground and expansion of tree PFTs, with the specific PFTs depending on location and altitude; the projected increase of tree coverage is dominated by temperate broadleaf deciduous trees in Tibetan Plateau, by both temperate broadleaf deciduous trees and shrubs in north China, and by tropical broadleaf deciduous trees in India. Over India, the expansion of tropical broadleaf deciduous trees is accompanied by a decrease of both bare ground and C4 grass cover. In general a shift of vegetation cover from bare ground to grass or from grass to trees is projected over most regions including the Tibetan Plateau, north China, southeast China, and India under all RCPs. Conversely, an opposite shift is projected

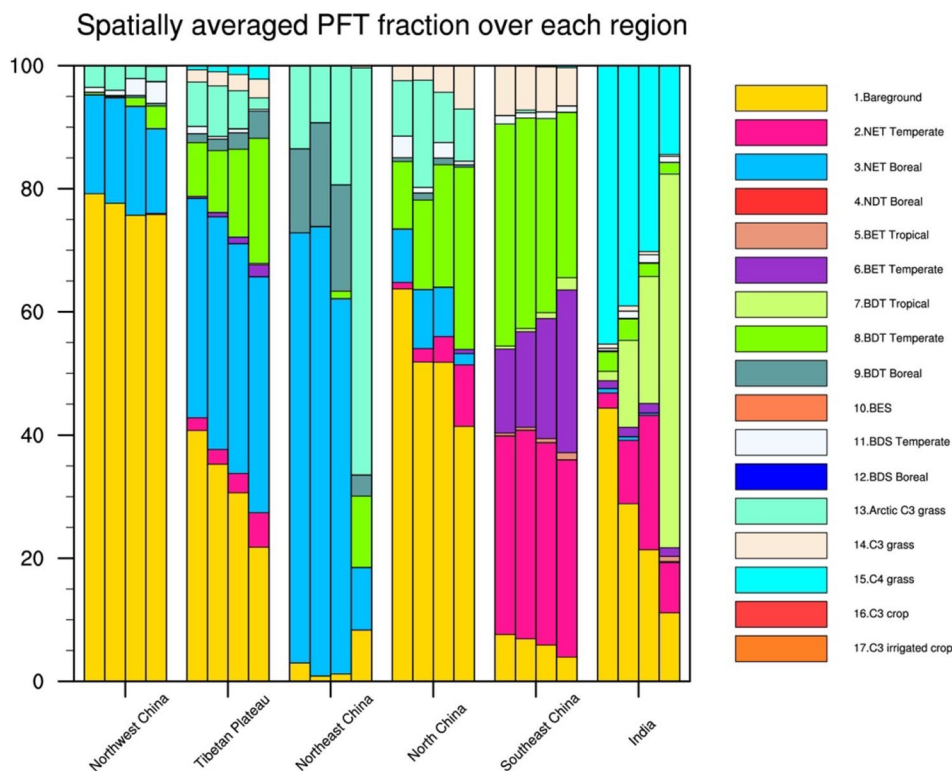


**Fig. 6** Spatially averaged PFT coverage (in %) in the six sub-regions, from RCM–CLM–CNDV historical and future scenario simulations. For each sub-region, the four columns (from left to right) represent historical, RCP2.6, RCP4.5 and RCP8.5, respectively. The segments in each bar (from top to bottom) represent up to 17 different PFTs: 1. Bare ground; 2. Needleleaf evergreen temperate tree; 3. Needleleaf evergreen boreal tree; 4. Needleleaf deciduous boreal tree; 5. Broad-

leaf evergreen tropical tree; 6. Broadleaf evergreen temperate tree; 7. Broadleaf deciduous tropical tree; 8. Broadleaf deciduous temperate tree; 9. Broadleaf deciduous boreal tree; 10. Broadleaf evergreen shrub; 11. Broadleaf deciduous temperate shrub; 12. Broadleaf deciduous boreal shrub; 13. Arctic C3 grass; 14. C3 grass; 15. C4 grass; 16. C3 crop; 17. C3 irrigated crop

under RCP8.5 for northeast China where trees would give way to Arctic C3 grass, and the projected decrease of woody plants coverage is dominated by a decrease of boreal needleleaf evergreen trees with minor contribution from a decrease of boreal broadleaf deciduous trees and shrubs.

The model can depict the seasonal variation of vegetation activities (Fig. 7), but with a delayed onset, peaking, and senescence of leaves in some regions. In most regions, the overestimation of LAI in the historical simulation (discussed earlier in Fig. 4) occurs in all seasons. As climate changes in the future, LAI would increase (with the largest increase in southeast China and India), and its seasonal cycle would remain similar in the future for most RCP scenarios and most regions (Fig. 7a, b, d–f). Notable exceptions are found in the RCP8.5 projection with substantially amplified seasonal contrast of LAI over Tibetan Plateau, north China, and India due to a projected increase of deciduous trees (Fig. 7b, d, f) and over northeast China due to the projected loss of evergreen trees (Fig. 7c).

Over most regions, the transition of vegetation from historical to low-, medium-, and high-emission scenarios

respectively is qualitatively similar, with gradual increase in the magnitude of changes as CO<sub>2</sub> emission increases. Exceptions are found over India and northeast China where the projected changes for high emission scenarios are dramatically different from those for lower emission scenarios (Figs. 5 and 6), indicating the likelihood of severe climate change crossing certain thresholds of vegetation competition. In the northeast China region, the projected loss of forest to grassland is primarily a result of heat stress caused by a large magnitude of warming during the growing season (Fig. 2), with some contribution from water stress. The dominantly needleleaf evergreen trees (as in the historical simulation) respond to heat stress with reduced gross primary productivity and increased background mortality. In addition, despite the projected increase of precipitation over most of the domain (Fig. 2), the warming-induced acceleration of ET (Figs 3a–f) and the increased summertime runoff (Fig. 3g–i) due to more intense precipitation together lead to a future decrease of soil moisture over a major portion of the domain including northeast China (Fig. 3j–l), exacerbating growing-season water stress. In the Indian region, the

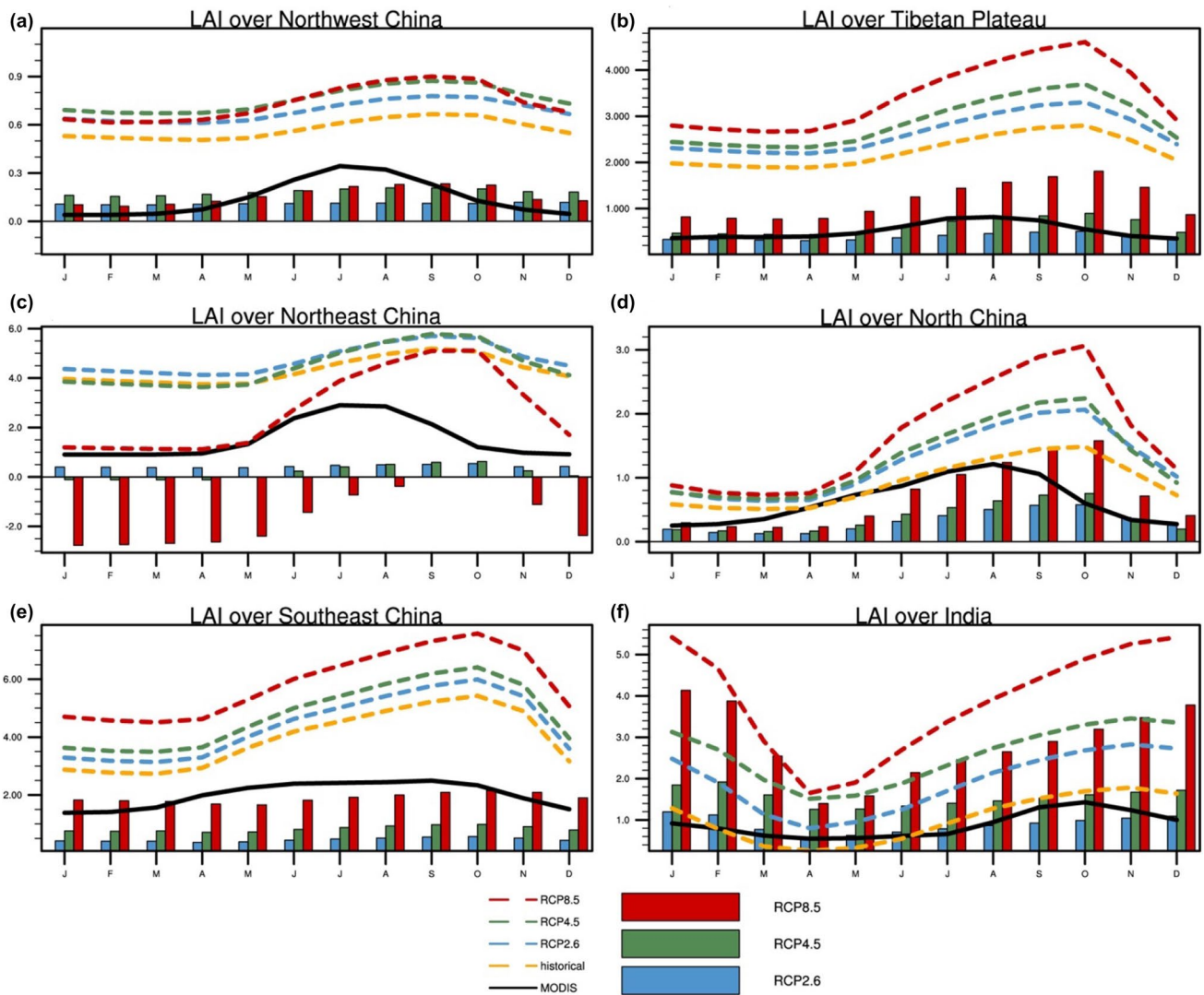


**Fig. 7** Seasonal cycle of LAI (units:  $\text{m}^2 \text{m}^{-2}$ ) spatially averaged over each sub-region from prescribed satellite (black line), RCM–CLM–CNDV historical and future RCPs simulations (orange, green, blue

and red lines), and the projected future changes compared to present-day simulation (green, blue and red bars). Only spatially averaged changes exceeding the two-tailed 95% confidence are shown

projected increase of precipitation amount is dominant over ET and runoff changes, leading to an increase of soil moisture (Fig. 3j–l), which diminishes water stress and favors tropical deciduous trees over grass.

### 3.3 Impact of dynamic vegetation feedback on surface climate change

The experimental design as described in Sect. 2 supports two different approaches to quantifying the dynamic vegetation feedback to regional climate. However, over most of the domain, results based on the two approaches are essentially the same. We therefore focus our description on results from the first approach; results from the second approach are presented in the supplementary file

(Supplementary Figs. 1–4). In addition, as most of the changes induced by vegetation feedback are not significant under RCP2.6 and RCP4.5, our results analysis here focuses on the RCP8.5 scenario.

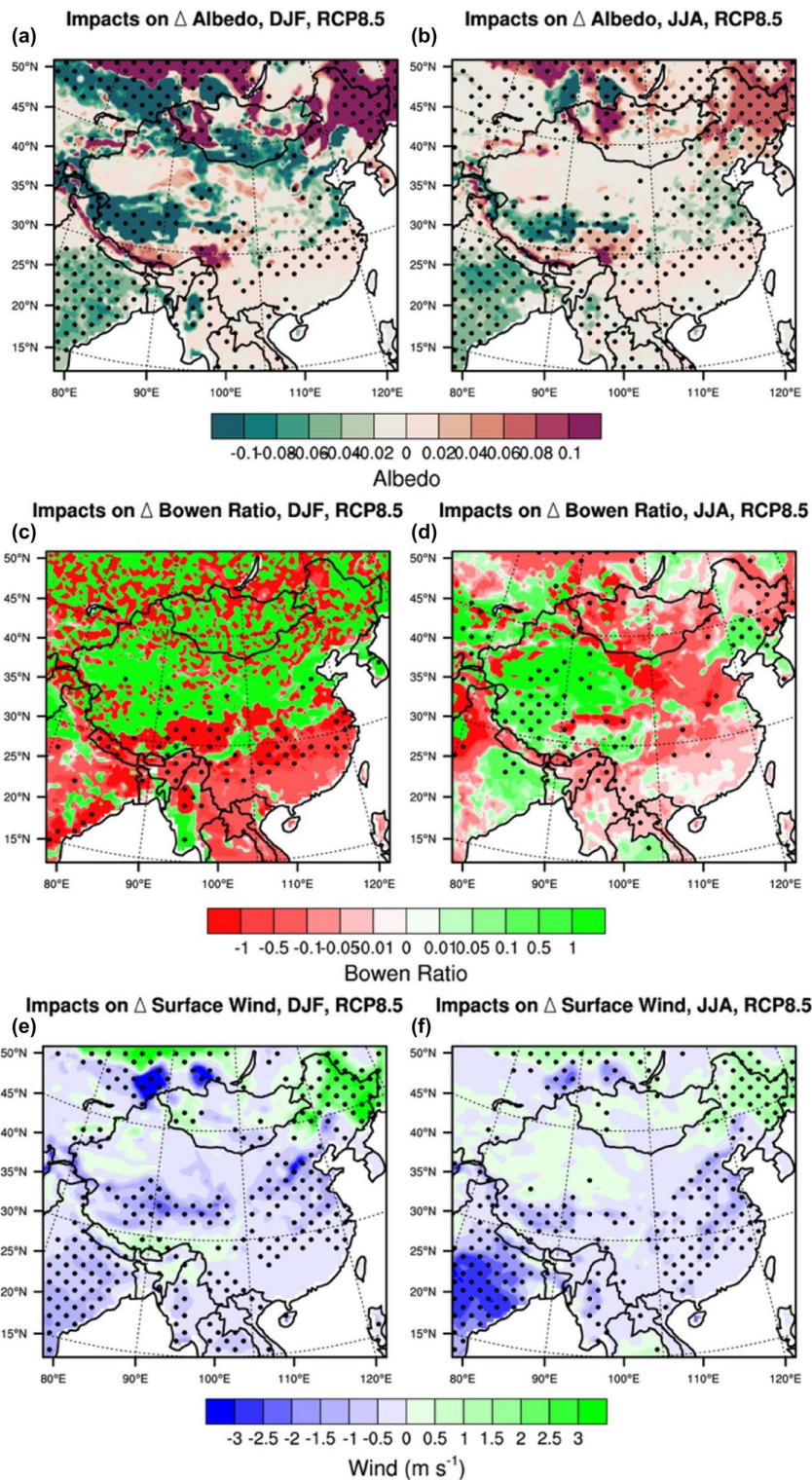
Vegetation influences regional climate through its impact on surface albedo, Bowen ratio, and roughness. Theoretically, when vegetation increases, albedo tends to decrease, Bowen ratio decrease, and surface roughness increase. Lower albedo leads to more shortwave absorption and more net radiation; lower Bowen ratio tends to increase latent heat flux and reduces sensible heat flux, while increased surface roughness tend to increase turbulent transport of both sensible and latent heat. The increased surface roughness also tends to slow down the surface wind. These processes and mechanisms interact and compete to shape the response of

the regional climate to vegetation changes, and some effects may offset each other.

Figure 8 shows the changes of the surface albedo, Bowen ratio, and surface wind speed attributed to the dynamic vegetation feedback under RCP8.5. Consistent with where the strongest vegetation changes are projected (Fig. 5), large,

statistically significant changes of albedo are projected primarily in northeast China with an increase due to the loss of forest, and in Tibetan Plateau and part of India with a decrease due to the expansion of vegetation cover (Fig. 8a, b). The response of Bowen ratio to vegetation feedback is more complex. In most of warm regions/seasons, Bowen

**Fig. 8** Impacts of vegetation feedback on surface albedo (top panel, units: 1), Bowen ratio (middle panel, units: 1) and surface wind (bottom panel, units:  $\text{m s}^{-1}$ ) changes in DJF (a–c) and JJA (d–f) under RCP8.5 scenario. Areas with values exceeding the two-tailed 95% confidence level with a  $t$  distribution are dotted



ratio is projected to decrease (Fig. 8d), largely as a result of the project increase of LAI, which is as expected; in cold regions/seasons, the Bowen ratio is subject to a high degree of uncertainty due to the small magnitude of latent heat flux (Fig. 8c), and the vegetation feedback signal is mixed. Over a major portion of western China, an increasing signal of Bowen ratio is likely a reflection of increased water stress limiting evapotranspiration. Across most of the domain, vegetation feedback causes a decrease of surface wind speed (Fig. 8e, f), consistent with an increase of roughness when vegetation becomes denser (with greater LAI).

Figure 9 shows the future vegetation-induced differences in surface net shortwave radiation, net radiation, and turbulent heat fluxes under RCP8.5. Not surprisingly, the largest differences are found primarily in regions where significant future changes of vegetation are projected, including for example the northeast China and India regions. The differences in net radiation (Fig. 9b, f) strongly resemble those for net shortwave radiation (Fig. 9a, e), reflecting the dominant role of albedo in surface net radiation changes, and the spatial pattern is remarkably similar between DJF and JJA. For example, in northeast China, the projected albedo increase (due to grass replacing trees) would cause both the surface net shortwave radiation (Fig. 9a, e) and surface net

radiation (Fig. 9b, f) to decrease significantly; in India, projected albedo decrease (due to trees replacing grass) would cause a significant increase of surface net shortwave and net radiation. The response of sensible heat flux (Fig. 9d, h) to the projected vegetation changes is similar to that of net radiation, except that the increase of sensible heat flux over India is stronger than the increase of net radiation in JJA and weaker in DJF. The response of latent heat flux (Fig. 9c, g) follows a spatial pattern similar to net radiation in northeast China, where latent heat flux (and ET) would slow down during all seasons due to the loss of tree coverage under RCP8.5. Over India during DJF, LAI is high (reaching 1.5 under historical and  $\sim 5.0$  under RCP8.5) and soil is still quite wet, so the tree coverage and LAI increases together with the net radiation increases (due to the lower albedo) cause a substantial increase of latent heat flux (ET). In JJA over India, vegetation feedback causes an increase of sensible heat flux (Fig. 9h) and a decrease of latent heat flux (Fig. 9g), which results from an interaction between the monsoon circulation and projected vegetation changes. Specifically, during the peak monsoon season in JJA, due to the frequent and heavy cloudiness, the albedo-induced increase of net radiation (Fig. 9f) is smaller than in DJF (Fig. 9b); on the other hand, the presence of cool and moist air brought

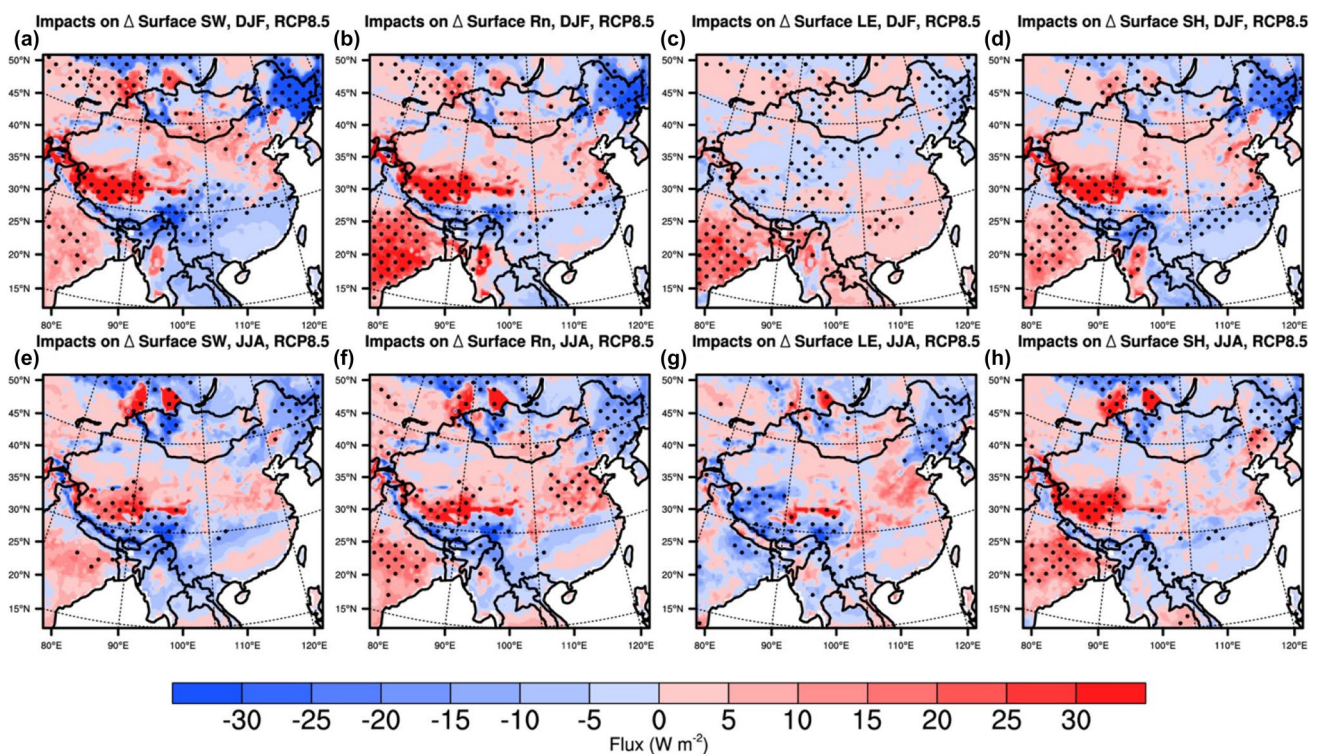


**Fig. 9** Impacts of vegetation feedback on surface net shortwave flux (SW, 1st column, units:  $\text{W m}^{-2}$ ), net radiation flux (Rn, 2nd column, units:  $\text{W m}^{-2}$ ), latent heat flux (LE, 3rd column, units:  $\text{W m}^{-2}$ ) and sensible heat flux (SH, 4th column, units:  $\text{W m}^{-2}$ ) changes in DJF (a–

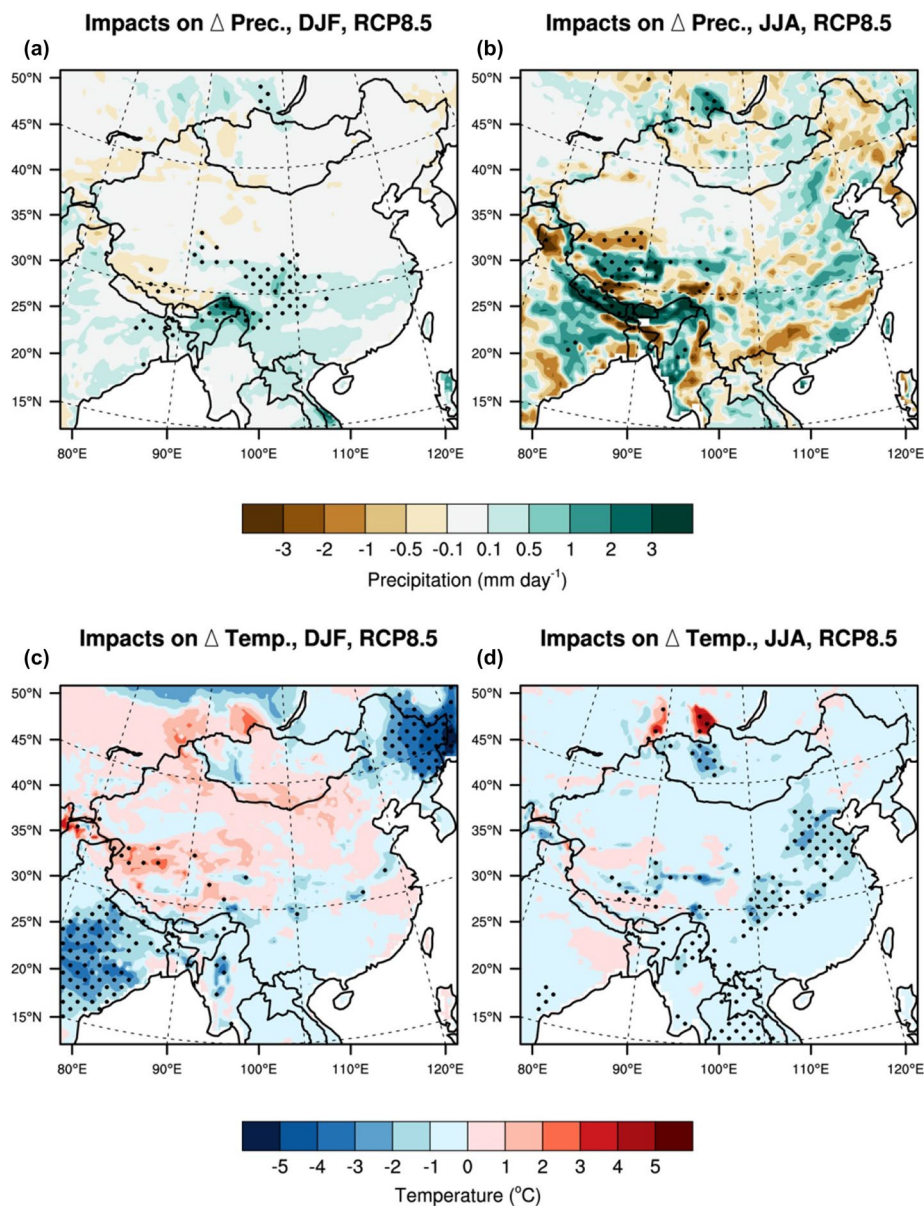
d) and JJA (e–h) under RCP8.5 scenario. Areas with values exceeding the two-tailed 95% confidence level with a *t* distribution are dotted

inland by the monsoon wind enhances the effects of surface roughness on sensible heat flux and weakens its effects on latent heat flux, which offsets the effects of vegetation-induced Bowen ratio changes. These two work together to reduce latent heat flux (ET) and increase sensible heat flux in this region when dynamic vegetation feedback is included (Fig. 9), which also causes the actual Bowen ratio to increase (Fig. 8).

Compared with projections by RCM–CLM with static vegetation, future climate changes projected by RCM–CLM–CNDV with dynamic vegetation follow similar spatial patterns and similar seasonality over most of the domain (figures not shown). Quantitatively, relative to the changes projected with static vegetation, dynamic vegetation feedback influences the projected climate changes (Fig. 10),

with the largest impact found primarily over regions where major vegetation changes are projected (e.g., Tibetan Plateau, northeast China and India). The impact on annual precipitation changes is dominated by changes during warm/wet seasons (e.g., JJA) with little contribution from the cold/dry seasons (Fig. 10a, b). For example, in northeast China where a forest-to-grassland transition and a decrease of LAI are projected for RCP8.5 (Fig. 5i–l), dynamic vegetation feedback leads to a significant decrease of ET and precipitation in RCP8.5, with most of the contribution from the warm season. As the model with static vegetation projects an increase of ET in northeast China (Fig. 3), the dry signal in northeast China indicates that land cover degradation (induced primarily by future heat stress in this study) tends to reduce both ET and precipitation in this region, a general notion supported

**Fig. 10** Impacts of vegetation feedback on changes in precipitation (top panel, units:  $\text{mm day}^{-1}$ ) and near surface air temperature (bottom panel, units:  $^{\circ}\text{C}$ ) in DJF (a–c) and JJA (b–d) under RCP8.5 scenario. Areas with values exceeding the two-tailed 95% confidence level with a t distribution are dotted



by many previous studies on vegetation feedback to precipitation in various regions of the globe (e.g., Wang and Eltahir 2000a, b; Wang et al. 2016; Lawrence and Vandecar 2015). Contrary to the seasonality of vegetation feedback on precipitation changes, the impact of vegetation feedback on annual mean temperature ( $T_{\text{mean}}$ ) changes (Fig. 10c, d) is dominated by the cold season (DJF), with much smaller impact during summer (JJA). In DJF (Fig. 10c), vegetation feedback would induce a statistically significant cooling impact ( $p < 0.05$ ) over both northeast China (as a result of albedo increase) and India (due to ET or latent heat flux increase dominant over albedo decrease). In JJA over most of the domain (Fig. 10d), the impact on temperature is weak and statistically not significant. In most regions, the magnitude of vegetation feedback on mean temperature (whether it is warming or cooling) is weak relative to the magnitude of projected GHG warming (Fig. 2g–l). Exceptions are found in the northeast China and India regions. For example, in northeast China under RCP8.5 (Fig. 10i), vegetation feedback significantly attenuates the projected warming during winter and spring, while the impact is negligible under RCP2.6 and RCP4.5. In India, the cooling effects due to vegetation feedback is strong

during winter and spring for all three RCPs, significantly curbing the projected warming in that region.

In general, vegetation feedback exerts a stronger impact on daytime high temperature ( $T_{\text{max}}$ ) and nighttime low temperature ( $T_{\text{min}}$ ) than on mean temperature ( $T_{\text{mean}}$ ), and the impacts on  $T_{\text{max}}$  and  $T_{\text{min}}$  may offset each other leading to a generally weak signal on projected  $T_{\text{mean}}$ . Although the wintertime cooling signal in  $T_{\text{mean}}$  is similar between northeast China and India under RCP8.5 (Fig. 10c), the impacts on  $T_{\text{max}}$  and  $T_{\text{min}}$  are different. Over northeast China (Fig. 11a–c), the albedo effect due to the loss of forest cover is dominant, causing a strong day-time cooling signal in  $T_{\text{max}}$  (Fig. 11b) that persists into the night to influence  $T_{\text{min}}$  (Fig. 11c), resulting in a decrease of  $T_{\text{mean}}$  (Fig. 11a). Over India, the warming effect of lower albedo due to forest expansion competes against the cooling effect of increased ET, leading to a weak warming signal in  $T_{\text{max}}$  at the time of the strongest solar radiation (Fig. 11e); the ET cooling effect appear to be dominant for the rest of the day when solar radiation is lower, leading to a cooling signal in  $T_{\text{min}}$  and  $T_{\text{mean}}$  (Fig. 11d, f).

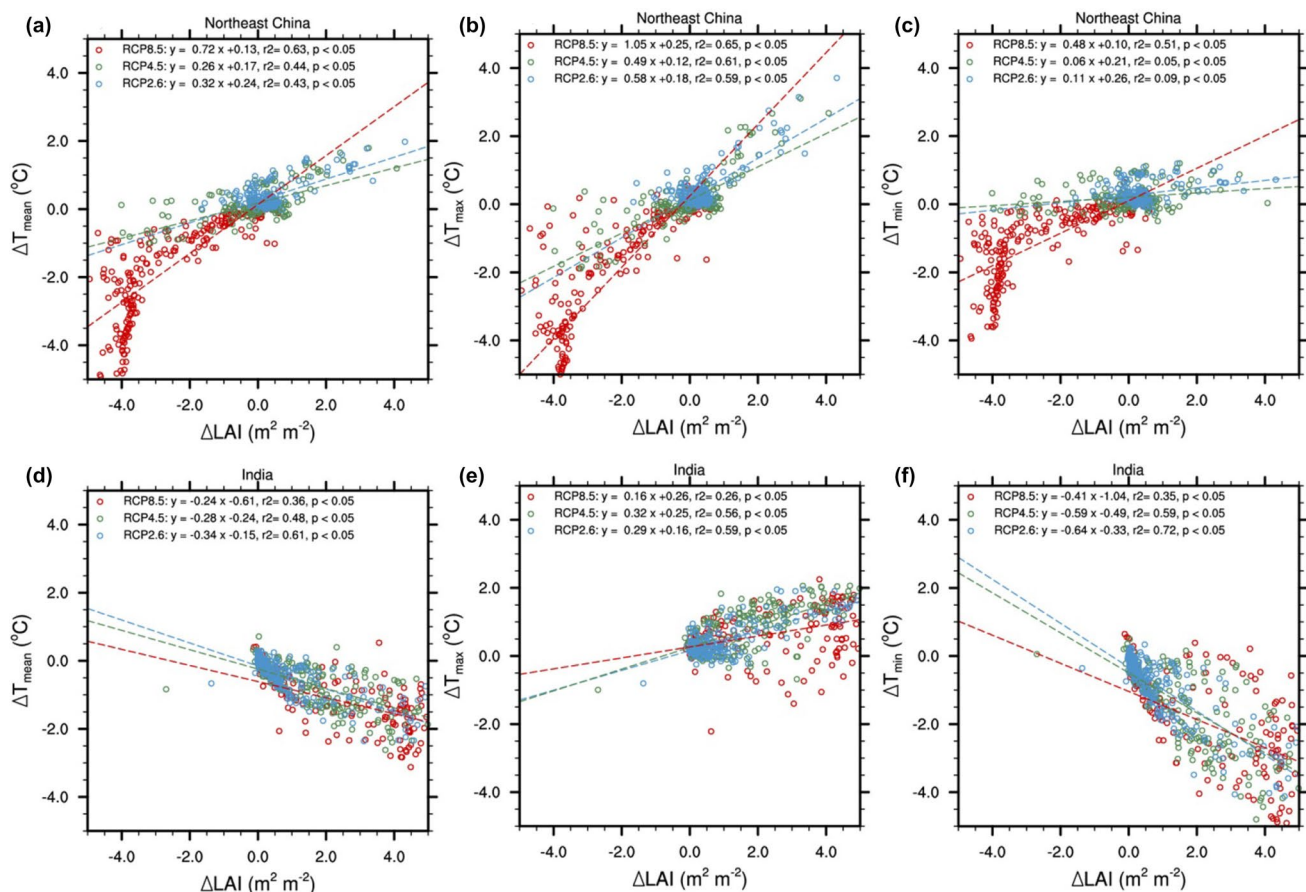


**Fig. 11** Spatial relationship between LAI changes and impacts of vegetation feedback on daily mean temperature (1st column), daily maximum temperature (2nd column) and daily minimum temperature (3rd column) in DJF over northeast China (a–c) and India (d–f) regions

## 4 Summary and discussion

Driven with lateral boundary conditions from FGOALS-g2, a regional climate model with static vegetation (RCM–CLM) and with dynamic vegetation (RCM–CLM–CNDV) is used in this study to assess future changes of the vegetation–climate system over East Asia, and to investigate the impacts of vegetation feedback on regional climate changes.

Over most of the region, the model projects a generally slight increase of vegetation cover accompanied by a significant increase of LAI, and the magnitude of these projected changes tends to increase gradually from low to high RCPs. Exceptions are found over two regions where major shift of vegetation is projected under RCP8.5, including India where trees would replace grassland and grass expand to historically bare ground due to increased water availability, and northeast China where grassland would replace needleleaf evergreen trees due to heat stress. The projected increases in vegetation cover and LAI are mainly due to the CO<sub>2</sub> fertilization effects and warming. Increase of heat stress, which triggers the crossing of a specific PFT threshold for mortality in the dynamic vegetation model, is the main cause for the projected vegetation changes in northeast China (which is the only major region of vegetation degradation accompanied by a strong decrease of LAI).

RCM–CLM projects a significant increase of temperature across the entire domain for all three RCPs. Over most of the domain, the projected warming is stronger during JJA than DJF, and the warming during JJA is stronger at mid- and high-latitudes than lower latitudes. Over most of the domain under all three RCPs, both ET and precipitation are projected to increase especially during JJA, as a result of warming-induced acceleration of the hydrological cycle; the signal is much weaker during DJF. Soil is projected to become wetter over north China and India where the increase of precipitation is dominant over ET, and become drier over the mid-latitudes where the projected warming is the strongest and the increase of ET is dominant over precipitation. The wetter soil in India directly leads to the expansion of trees there, and the drier soil in northeast China partly contributes to the loss of forest to grassland.

Climate projections from RCM–CLM–CNDV and RCM–CLM show a similar spatial pattern, but the two differ significantly over regions where large changes of vegetation are projected under RCP8.5. The differences in projected precipitation changes are mostly small, while differences in ET and temperature projections are more significant and widespread. In northeast China, dynamic vegetation feedback causes a lower ET in RCM–CLM–CNDV

than in RCM–CLM during both DJF and JJA, due to the loss of forest to grassland. In India where an expansion of vegetation cover is projected, ET during DJF is higher in RCM–CLM–CNDV than in RCM–CLM. However, in India during JJA, dynamic vegetation feedback causes ET to be lower, as the increased surface roughness favors sensible heat flux over latent heat flux due to the presence of cool and moist air brought in by the monsoon wind. For temperature, dynamic vegetation feedback causes a strong and significant cooling during DJF over both northeast China (due to the albedo effect) and India (due to the surface roughness and Bowen ratio effects). Dynamic vegetation feedback exerts a stronger impact on daytime high ( $T_{\max}$ ) and nighttime low ( $T_{\min}$ ) than on mean temperature ( $T_{\text{mean}}$ ) over areas where substantial vegetation changes are projected.

Findings from this study are subject to uncertainties from several sources, including for example the model's inability to simulate managed ecosystem and lack of consideration for irrigation (both of which influence regional climate) as well as underestimation of precipitation and temperature (that influences the growth of vegetation). For example the north China Plain is dominated by irrigated cropland in reality, but the modeled potential natural vegetation for this region is bare ground, which affects climate quite differently from irrigated crops (Kang and Eltahir 2018). Moreover, afforestation over north China and agriculture over India were suggested to have contributed to the global greening observed by satellites (Chen et al. 2019). These anthropogenic vegetation changes (and their impact on regional climate) are not accounted for by the coupled vegetation–climate model used here.

The results of this study is based on one of the CMIP5 models that show good performance over East Asia, so the GCM-related uncertainties are not sampled. In the particular model chosen, changes under RCP8.5 are large enough to cross certain biophysical or physiological thresholds. Based on projections for the northeast China region in particular, boreal forests are likely very vulnerable in the future; some of the changes might be irreversible and could exacerbate the GHG-induced climate changes. Given the drastically different projections among the multiple emission scenarios (especially in northeast China and India), the level of RCP-related uncertainty is high. The results under high emission scenarios should be further tested using an ensemble of RCM experiments driven by multiple GCMs. Dynamic vegetation modeling is another source of uncertainty. DGVMs typically produce exaggerated changes due to the lack of consideration for plant migration and seed dispersal (Higgins and Harte, 2006); likely such changes will take a much longer time to occur than projected by the model (Lehsten et al. 2019).

**Acknowledgements** This study was made possible by a scholarship from the China Scholarship Council that supported Weiguang Liu's visit to the University of Connecticut. Computational support was made available through an NCAR computing project to the University of Connecticut (UCNN0017). Yu, Chen and Shi were supported by the National Natural Science Foundation of China (41575084, 41625019 and 41805063). Liu acknowledges funding support by the Postgraduate Research and Practice Innovation Program of Jiangsu Province (KYCX18\_1013). The authors thank Michael Notaro for his constructive comments on an earlier version of this paper.

## References

- Alkama R, Cescatti A (2016) Biophysical climate impacts of recent changes in global forest cover. *Science* 351:600–604. <https://doi.org/10.1126/science.aac8083>
- Alo CA, Wang G (2008) Potential future changes of the terrestrial ecosystem based on climate projections by eight general circulation models. *J Geophys Res-Biogeophys*. <https://doi.org/10.1029/2007jg000528>
- Betts RA (2000) Offset of the potential carbon sink from boreal forestation by decreases in surface albedo. *Nature* 408:187–190. <https://doi.org/10.1038/35041545>
- Bonan GB (2008) Forests and climate change: forcings, feedbacks, and the climate benefits of forests. *Science* 320:1444–1449. <https://doi.org/10.1126/science.1155121>
- Bonan GB, Doney SC (2018) Climate, ecosystems, and planetary futures: the challenge to predict life in Earth system models. *Science* 359:eaam8328. <https://doi.org/10.1126/science.aam8328>
- Charney JG (1975) Dynamics of deserts and drought in the Sahel. *Q J R Meteor Soc* 101:193–202. <https://doi.org/10.1002/qj.49710142802>
- Chen C et al (2019) China and India lead in greening of the world through land-use management. *Nat Sustain* 2:122–129. <https://doi.org/10.1038/s41893-019-0220-7>
- Cox PM, Betts RA, Jones CD, Spall SA, Totterdell IJ (2000) Acceleration of global warming due to carbon-cycle feedbacks in a coupled climate model. *Nature* 408:184–187. <https://doi.org/10.1038/35041539>
- Cramer W et al (2001) Global response of terrestrial ecosystem structure and function to CO<sub>2</sub> and climate change: results from six dynamic global vegetation models. *Glob Chang Biol* 7:357–373. <https://doi.org/10.1046/j.1365-2486.2001.00383.x>
- Dan L, Cao F, Gao R (2015) The improvement of a regional climate model by coupling a land surface model with eco-physiological processes: a case study in 1998. *Clim Change* 129:457–470. <https://doi.org/10.1007/s10584-013-0997-8>
- Davin EL, de Noblet-Ducoudré N (2010) Climatic impact of global-scale deforestation: radiative versus nonradiative processes. *J Clim* 23:97–112. <https://doi.org/10.1175/2009JCLI3102.1>
- Duveiller G, Hooker J, Cescatti A (2018) The mark of vegetation change on Earth's surface energy balance. *Nat Commun* 9:679. <https://doi.org/10.1038/s41467-017-02810-8>
- Emanuel KA (1991) A scheme for representing cumulus convection in large-scale models. *J Atmos Sci* 48:2313–2329. [https://doi.org/10.1175/1520-0469\(1991\)048%3c2313:Asfrce%3e2.0.Co;2](https://doi.org/10.1175/1520-0469(1991)048%3c2313:Asfrce%3e2.0.Co;2)
- Erfanian A, Wang G (2018) Explicitly accounting for the role of remote oceans in regional climate modeling of South America. *J Adv Model Earth Syst* 10:2408–2426. <https://doi.org/10.1029/2018ms001444>
- Erfanian A, Wang G, Yu M, Anyah R (2016) Multimodel ensemble simulations of present and future climates over West Africa: impacts of vegetation dynamics. *J Adv Model Earth Syst* 8:1411–1431. <https://doi.org/10.1002/2016MS000660>
- Franklin J, Serra-Diaz JM, Syphard AD, Regan HM (2016) Global change and terrestrial plant community dynamics. *Proc Natl Acad Sci USA* 113:3725–3734. <https://doi.org/10.1073/pnas.1519911113>
- Gang C et al (2017) Modeling the dynamics of distribution, extent, and NPP of global terrestrial ecosystems in response to future climate change. *Glob Planet Change* 148:153–165. <https://doi.org/10.1016/j.gloplacha.2016.12.007>
- Gao X, Xu Y, Zhao Z, Pal JS, Giorgi F (2006) On the role of resolution and topography in the simulation of East Asia precipitation. *Theor Appl Climatol* 86:173–185. <https://doi.org/10.1007/s00704-005-0214-4>
- Gibbard S, Caldeira K, Bala G, Phillips T, Wickett M (2005) Climate effects of global land cover change. *Geophys Res Lett*. <https://doi.org/10.1029/2005GL024550>
- Giorgi F et al (2012) RegCM4: model description and preliminary tests over multiple CORDEX domains. *Clim Res* 52:7–29. <https://doi.org/10.3354/cr01018>
- Gotangco Castillo CK, Levis S, Thornton P (2012) Evaluation of the new CNDV option of the community land model: effects of dynamic vegetation and interactive nitrogen on CLM4 means and variability\*. *J Clim* 25:3702–3714. <https://doi.org/10.1175/jcli-d-11-00372.1>
- He C, Zhou T (2015) Responses of the Western North Pacific subtropical high to global warming under RCP4.5 and RCP8.5 scenarios projected by 33 CMIP5 models: the dominance of tropical Indian ocean-tropical Western Pacific SST gradient. *J Clim* 28:365–380. <https://doi.org/10.1175/jcli-d-13-00494.1>
- Henderson-Sellers A, Dickinson RE, Durbidge TB, Kennedy PJ, McGuffie K, Pitman AJ (1993) Tropical deforestation: modeling local- to regional-scale climate change. *J Geophys Res-Atmos* 98:7289–7315. <https://doi.org/10.1029/92jd02830>
- Higgins PAT, Harte J (2006) Biophysical and biogeochemical responses to climate change depend on dispersal and migration. *BioScience*. [https://doi.org/10.1641/0006-3568\(2006\)056%5b0407: Babrtc%5d2.0.Co;2](https://doi.org/10.1641/0006-3568(2006)056%5b0407: Babrtc%5d2.0.Co;2)
- Holtslag AAM, De Bruijn EIF, Pan HL (1990) A high resolution air mass transformation model for short-range weather forecasting. *Mon Weather Rev* 118:1561–1575. [https://doi.org/10.1175/1520-0493\(1990\)118%3c1561:Ahramt%3e2.0.Co;2](https://doi.org/10.1175/1520-0493(1990)118%3c1561:Ahramt%3e2.0.Co;2)
- Hua W, Chen H, Sun S, Zhou L (2015) Assessing climatic impacts of future land use and land cover change projected with the CanESM2 model. *Int J Climatol* 35:3661–3675. <https://doi.org/10.1002/joc.4240>
- Hua W et al (2017) Observational quantification of climatic and human influences on vegetation greening in China. *Remote Sens*. <https://doi.org/10.3390/rs9050425>
- IPCC (2013) Climate change 2013: the physical science basis. In: Stocker TF et al (eds) Contribution of working group I to the fifth assessment report of the intergovernmental panel on climate change. Cambridge University Press, Cambridge
- Jeong SJ, Ho CH, Jeong JH (2009a) Increase in vegetation greenness and decrease in springtime warming over east Asia. *Geophys Res Lett*. <https://doi.org/10.1029/2008GL036583>
- Jeong SJ, Ho CH, Kim KY, Jeong JH (2009b) Reduction of spring warming over East Asia associated with vegetation feedback. *Geophys Res Lett*. <https://doi.org/10.1029/2009GL039114>
- Kang S, Eltahir EAB (2018) north China Plain threatened by deadly heatwaves due to climate change and irrigation. *Nat Commun* 9:2894. <https://doi.org/10.1038/s41467-018-05252-y>
- Kiehl JT, Hack JJ, Bonan GB, Boville BA, Briegleb BP, Williamson DL, Rasch PJ (1996) Description of the NCAR community climate model (ccm3). <https://doi.org/10.5065/D6FF3Q99>
- Lawrence PJ, Chase TN (2007) Representing a new MODIS consistent land surface in the Community Land Model (CLM 3.0). *J Geophys Res* 112:252–257. <https://doi.org/10.1029/2006jg000168>

- Lawrence D, Vandecar K (2015) Effects of tropical deforestation on climate and agriculture. *Nat Clim Change* 5:27–36. <https://doi.org/10.1038/nclimate2430>
- Lawrence DM et al (2011) Parameterization improvements and functional and structural advances in version 4 of the community land model. *J Adv Model Earth Syst*. <https://doi.org/10.1029/2011M500045>
- Lehsten V, Mischurow M, Lindström E, Lehsten D, Lischke H (2019) LPJ-GM 1.0: simulating migration efficiently in a dynamic vegetation model. *Geosci Model Dev* 12:893–908. <https://doi.org/10.5194/gmd-12-893-2019>
- Li L et al (2013) The flexible global ocean-atmosphere-land system model, Grid-point Version 2: FGOALS-g2. *Adv Atmos Sci* 30:543–560. <https://doi.org/10.1007/s00376-012-2140-6>
- Li Y, Zhao M, Motesharrei S, Mu Q, Kalnay E, Li S (2015) Local cooling and warming effects of forests based on satellite observations. *Nat Commun* 6:6603. <https://doi.org/10.1038/ncomms7603>
- Li D, Zhou T, Zou L, Ma S (2016) Simulated and projected surface air temperature over China in RegCM3 CORDEX East Asia experiments. *Chin J Atmos Sci (in Chinese)* 41:544–560. <https://doi.org/10.3878/j.issn.1006-9895.1607.16153>
- Li X et al (2017) Potential effects of land cover change on temperature extremes over Eurasia: current versus historical experiments. *Int J Climatol* 37:59–74. <https://doi.org/10.1002/joc.4976>
- Li D, Zou L, Zhou T (2018) Extreme climate event changes in China in the 1.5 and 2 & #x0;C warmer climates: results from statistical and dynamical downscaling. *J Geophys Res-Atmos* 123:10215–10230. <https://doi.org/10.1029/2018jd028835>
- Liu Y, Stanturf J, Lu H (2008) Modeling the potential of the Northern China forest shelterbelt in improving hydroclimate conditions. *JAWRA* 44:1176–1192. <https://doi.org/10.1111/j.1752-1688.2008.00240.x>
- Ma D, Notaro M, Liu Z, Chen G, Liu Y (2013) Simulated impacts of afforestation in East China monsoon region as modulated by ocean variability. *Clim Dyn* 41:2439–2450. <https://doi.org/10.1007/s00382-012-1592-9>
- Mahowald N, Lo F, Zheng Y, Harrison L, Funk C, Lombardozzi D, Goodale C (2016) Projections of leaf area index in earth system models. *Earth Syst Dyn* 7:211–229. <https://doi.org/10.5194/esd-7-211-2016>
- Mao J et al (2016) Human-induced greening of the northern extratropical land surface. *Nat Clim Change* 6:959–963. <https://doi.org/10.1038/nclimate3056>
- Melillo J, McGuire D, Kicklighter DW, Moore B, Vorosmarty C, Schloss AL (1993) Global climate change and terrestrial net primary production. *Nature* 363:234–240. <https://doi.org/10.1038/363234a0>
- Moss RH et al (2010) The next generation of scenarios for climate change research and assessment. *Nature* 463:747–756. <https://doi.org/10.1038/nature08823>
- Murray-Tortarolo G et al (2013) Evaluation of land surface models in reproducing satellite-derived LAI over the high-latitude northern hemisphere. Part I: uncoupled DGVMs. *Remote Sens* 5:4819–4838. <https://doi.org/10.3390/rs5104819>
- Nemani RR et al (2003) Climate-driven increases in global terrestrial net primary production from 1982 to 1999. *Science* 300:1560–1563. <https://doi.org/10.1126/science.1082750>
- Niu X, Tang J, Wang S, Fu C (2018) Impact of future land use and land cover change on temperature projections over East Asia. *Clim Dyn*. <https://doi.org/10.1007/s00382-018-4525-4>
- Notaro M, Liu Z (2008) Statistical and dynamical assessment of vegetation feedbacks on climate over the boreal forest. *Clim Dyn* 31:691–712. <https://doi.org/10.1007/s00382-008-0368-8>
- Notaro M, Chen G, Liu Z (2011) Vegetation feedbacks to climate in the global monsoon regions\*. *J Clim* 24:5740–5756. <https://doi.org/10.1175/2011jcli4237.1>
- Notaro M, Chen G, Yu Y, Wang F, Tawfik A (2017) Regional climate modeling of vegetation feedbacks on the Asian–Australian monsoon systems. *J Clim* 30:1553–1582. <https://doi.org/10.1175/JCLI-D-16-0669.1>
- Oleson KW et al (2010) Technical description of version 4.0 of the Community Land Model (CLM). NCAR Technical Note NCAR/TN-478+STR. <https://doi.org/10.5065/d6fb50wz>
- Oleson K et al (2013) Technical description of version 4.5 of the Community Land Model (CLM). Near Technical Note NCAR/TN-503+STR. <https://doi.org/10.5065/d6rr1w7m>
- Peng S et al (2013) Asymmetric effects of daytime and night-time warming on Northern Hemisphere vegetation. *Nature* 501:88. <https://doi.org/10.1038/nature12434>
- Shen M et al (2015) Evaporative cooling over the Tibetan Plateau induced by vegetation growth. *Proc Natl Acad Sci USA* 112:9299–9304. <https://doi.org/10.1073/pnas.1504418112>
- Shi Y, Wang G, Gao X (2017) Role of resolution in regional climate change projections over China. *Clim Dyn* 51:2375–2396. <https://doi.org/10.1007/s00382-017-4018-x>
- Shi Y, Yu M, Erfanian A, Wang G (2018) Modeling the dynamic vegetation–climate system over china using a coupled regional model. *J Clim* 31:6027–6049. <https://doi.org/10.1175/jcli-d-17-0191.1>
- Taylor KE, Stouffer RJ, Meehl GA (2012) An overview of CMIP5 and the experiment design. *Bull Am Meteor Soc* 93:485–498. <https://doi.org/10.1175/bams-d-11-00094.1>
- Tharammal T, Bala G, Narayanappa D, Nemani R (2018) Potential roles of CO<sub>2</sub> fertilization, nitrogen deposition, climate change, and land use and land cover change on the global terrestrial carbon uptake in the twenty-first century. *Clim Dyn* 52:4393–4406. <https://doi.org/10.1007/s00382-018-4388-8>
- Wang L, Chen W (2014) A CMIP5 multimodel projection of future temperature, precipitation, and climatological drought in China. *Int J Climatol* 34:2059–2078. <https://doi.org/10.1002/joc.3822>
- Wang G, Eltahir EA (2000a) Ecosystem dynamics and the Sahel Drought. *Geophys Res Lett* 27:795–798. <https://doi.org/10.1029/1999gl011089>
- Wang G, Eltahir EA (2000b) Role of vegetation dynamics in enhancing the low-frequency variability of the Sahel rainfall. *Water Resour Res* 36:1013–1021. <https://doi.org/10.1029/1999WR900361>
- Wang G, Eltahir EAB, Foley JA, Pollard D, Levis S (2004) Decadal variability of rainfall in the Sahel: results from the coupled GENESIS-IBIS atmosphere-biosphere model. *Clim Dyn* 22:625–637. <https://doi.org/10.1007/s00382-004-0411-3>
- Wang G, Yu M, Pal JS, Mei R, Bonan GB, Levis S, Thornton PE (2016) On the development of a coupled regional climate–vegetation model RCM–CLM–CN–DV and its validation in Tropical Africa. *Clim Dyn* 46:515–539. <https://doi.org/10.1007/s00382-015-2596-z>
- Wang G, Ahmed KF, You L, Yu M, Pal J, Ji Z (2017) Projecting regional climate and cropland changes using a linked biogeophysical-socioeconomic modeling framework: 1. Model description and an equilibrium application over West Africa. *J Adv Model Earth Syst* 9:354–376. <https://doi.org/10.1002/2016ms000712>
- Wei J, Jin Q, Yang Z-L, Zhou L (2017) Land-atmosphere-aerosol coupling in north China during 2000–2013. *Int J Climatol* 37:1297–1306. <https://doi.org/10.1002/joc.4993>
- Williams JW, Jackson ST, Kutzbach JE (2007) Projected distributions of novel and disappearing climates by 2100 AD. *Proc Natl Acad Sci USA* 104:5738–5742. <https://doi.org/10.1073/pnas.0606292104>
- Xue Y, Shukla J (1993) The influence of land surface properties on sahel climate. Part 1: desertification. *J Clim* 6:2232–2243. [https://doi.org/10.1175/1520-0442\(1993\)006%3c2232:TIOLS%3e2.0.CO;2](https://doi.org/10.1175/1520-0442(1993)006%3c2232:TIOLS%3e2.0.CO;2)
- Xue Y, De Sales F, Vasic R, Mechoso CR, Arakawa A, Prince S (2010) Global and seasonal assessment of interactions between climate

- and vegetation biophysical processes: a GCM study with different land–vegetation representations. *J Clim* 23:1411–1433. <https://doi.org/10.1175/2009jcli3054.1>
- Yan Y, Tang J, Liu G, Wu J (2019) Effects of vegetation fraction variation on regional climate simulation over Eastern China. *Glob Planet Change* 175:173–189. <https://doi.org/10.1016/j.gloplacha.2019.02.004>
- Yang W, Long D, Bai P (2019) Impacts of future land cover and climate changes on runoff in the mostly afforested river basin in North China. *J Hydrol* 570:201–219. <https://doi.org/10.1016/j.jhydrol.2018.12.055>
- Yao R, Wang L, Huang X, Chen X, Liu Z (2019) Increased spatial heterogeneity in vegetation greenness due to vegetation greening in mainland China. *Ecol Ind* 99:240–250. <https://doi.org/10.1016/j.ecolind.2018.12.039>
- Yu E, Wang H, Sun J, Gao Y (2013) Climatic response to changes in vegetation in the Northwest Hetao Plain as simulated by the WRF model. *Int J Climatol* 33:1470–1481. <https://doi.org/10.1002/joc.3527>
- Yu M, Wang G, Parr D, Ahmed KF (2014) Future changes of the terrestrial ecosystem based on a dynamic vegetation model driven with RCP8.5 climate projections from 19 GCMs. *Clim Change* 127:257–271. <https://doi.org/10.1007/s10584-014-1249-2>
- Yu M, Wang GL, Chen HS (2016a) Quantifying the impacts of land surface schemes and dynamic vegetation on the model dependency of projected changes in surface energy and water budgets. *J Adv Model Earth Syst* 8:370–386. <https://doi.org/10.1002/2015ms000492>
- Yu M, Wang G, Pal JS (2016b) Effects of vegetation feedback on future climate change over West Africa. *Clim Dyn* 46:1–20. <https://doi.org/10.1007/s00382-015-2795-7>
- Yu Y, Notaro M, Wang F, Mao J, Shi X, Wei Y (2017) Observed positive vegetation-rainfall feedbacks in the Sahel dominated by a moisture recycling mechanism. *Nat Commun* 8:1873. <https://doi.org/10.1038/s41467-017-02021-1>
- Zeng N, Neelin JD, Lau K-M, Tucker CJ (1999) Enhancement of interdecadal climate variability in the Sahel by vegetation interaction. *Science* 286:1537–1540. <https://doi.org/10.1126/science.286.5444.1537>
- Zeng Z et al (2018) Global terrestrial stilling: does Earth's greening play a role? *Environ Res Lett*. <https://doi.org/10.1088/1748-9326/aaea84>
- Zhao W, Hu Z, Guo Q, Wu G, Chen R, Li S (2019) Contributions of climatic factors to inter-annual variability of vegetation index in northern China grasslands. *J Clim*. <https://doi.org/10.1175/jcli-d-18-0587.1>
- Zhou L, Dickinson RE, Tian Y, Vose RS, Dai Y (2007) Impact of vegetation removal and soil aridation on diurnal temperature range in a semiarid region: application to the Sahel. *Proc Natl Acad Sci USA* 104:17937–17942. <https://doi.org/10.1073/pnas.0700290104>
- Zhou T, Song F, Chen X (2013) Historical evolution of global and regional surface air temperature simulated by FGOALS-s2 and FGOALS-g2: how reliable are the model results? *Adv Atmos Sci* 30:638–657. <https://doi.org/10.1007/s00376-013-2205-1>
- Zhu Z et al (2016) Greening of the Earth and its drivers. *Nat Clim Change* 6:791–795. <https://doi.org/10.1038/nclimate3004>
- Zou L, Zhou T (2013) Near future (2016–40) summer precipitation changes over China as projected by a regional climate model (RCM) under the RCP8.5 emissions scenario: comparison between RCM downscaling and the driving GCM. *Adv Atmos Sci* 30:806–818. <https://doi.org/10.1007/s00376-013-2209-x>

**Publisher's Note** Springer Nature remains neutral with regard to jurisdictional claims in published maps and institutional affiliations.